Revealing the Impact of Ferromagnetic Elements on Fe-Based Amorphous Alloy Properties via *ab initio* Molecular Dynamics Simulations and Experiments

Jin-Hua Xiao(肖晋桦)[1], Da-Wei Ding(丁大伟)[2*], Lin Li(李琳)[1], Yi-Tao Sun(孙奕韬)[2], Mao-Zhi Li(李茂枝)[3], and Wei-Hua Wang(汪卫华)[2]

[1]*State Key Laboratory of Alternate Electrical Power System with Renewable Energy Sources, North China Electric Power University, Beijing 102206, China*
[2]*Institute of Physics, Chinese Academy of Sciences, Beijing 100190, China*
[3]*Department of Physics and Beijing Key Laboratory of Opto-electronic Functional Materials & Micro-nano Devices, Renmin University of China, Beijing 100872, China*

(Received 30 October 2024; accepted manuscript online 12 December 2024)

A high saturation magnetic flux density (B_s) is essential for the development of Fe-based amorphous alloys for electromagnetic devices and motors. However, achieving a high B_s often compromises the glass-forming ability (GFA) of Fe-based amorphous alloys. This study investigates the effects of ferromagnetic elements (Fe, Co, and Ni) on the microstructure and magnetic properties of $Fe_{86}B_7C_7$ amorphous alloys through experiments and *ab initio* molecular dynamics simulations. By analyzing both the experimental and simulation results, the relationship between the atomic structures, GFA, and magnetic properties of these amorphous alloys was determined. The results indicate that the GFA of the alloys is correlated with the proportion of icosahedral and body-centered cubic clusters. The addition of Co and Ni not only improved the GFA of the alloys but also effectively increased the overall magnetic moment with an appropriate amount of Co and a small amount of Ni. This increase in the magnetic moment primarily arises from the enhancement of the magnetic moment of Fe atoms, resulting from the redistribution between the spin-up and spin-down electrons of Fe-3*d* orbits, as well as the strong exchange interactions between Fe and Co and Fe–Ni pairs. The results obtained offer valuable insights into the correlation between the atomic structure and magnetic properties of these amorphous alloys and suggest potential directions for the optimization of Fe-based amorphous alloys.

DOI: 10.1088/0256-307X/42/1/016102 CSTR: 32039.14.0256-307X.42.1.016102

Amorphous alloys, which are novel soft magnetic materials, have extensive applications in electromagnetic equipment and motors owing to their exceptional magnetic properties.[1–5] In comparison with conventional silicon steel, Fe-based amorphous alloys exhibit significant advantages in terms of core loss and energy conversion efficiency, making them promising alternatives to core materials in distribution transformers.[6] However, the saturation flux density (B_s) of amorphous alloys is still lower than that of silicon steel (approximately 2.0 T); for example, the B_s of the commercial amorphous alloy METGLAS 2605SA1 is only 1.56 T.[7] Recent research has shown that micro-alloying and optimization of the production process can enhance the magnetic properties of Fe-based amorphous alloys.[8] However, the improvement in magnetic properties often comes at the expense of reduced glass-forming ability (GFA).[9–11] Consequently, the trade-off between B_s and GFA in Fe-based amorphous alloys remains a major challenge.[12–14]

Previous studies demonstrated that the addition of appropriate amounts of Co to Fe-based amorphous alloys can effectively enhance B_s.[15,16] For instance, Inoue *et al.* successfully synthesized an alloy with a B_s value as high as 1.92 T and an H_c value of only 2 A/m by incorporating Co into high-Fe content amorphous alloys.[17] In addition, some studies have indicated that the addition of Ni to Fe-based amorphous alloys enhances their GFA and mechanical properties.[18] However, the addition of Ni may lead to a reduction in B_s and adversely affect the magnetic properties of the alloy.[19] Although these experimental studies optimized the properties of Fe-based amorphous alloys, the theoretical basis for the microstructural changes in these alloys caused by doping with ferromagnetic elements remains unclear. In recent years, *ab initio* molecular dynamics (AIMD) simulations have provided valuable insights into the micro-structures of amorphous alloys.[20–23] AIMD simulations have revealed that doping with Co and Ni can enhance the exchange splitting energy, thereby increasing the magnetic moment of the Fe atoms.[24,25] Research combining AIMD simulations with experimental results might further promote advancements in the material design of amorphous soft magnetic materials.[26] In particular, whether Ni doping can enhance the B_s of Fe-based amorphous alloys warrants systematic investigation. Therefore, it is crucial to systematically investigate the effects of ferromagnetic elements on the atomic structure

*Corresponding author. Email: dingdawei@iphy.ac.cn
© 2025 Chinese Physical Society and IOP Publishing Ltd. All rights, including for text and data mining, AI training, and similar technologies, are reserved.

and magnetism of Fe-based amorphous alloys, particularly when co-doped with Co and Ni.

This study investigates the effects of ferromagnetic elements (Fe, Co, and Ni) on the atomic structures and magnetic properties of $Fe_{86}B_7C_7$-based amorphous alloys using experimental methods and AIMD simulations. The results elucidate the mechanisms by which Co and Ni enhance the GFA of alloys from an atomic structure perspective. Furthermore, minor Ni doping was shown to effectively increase the magnetic moment of Fe atoms, and this finding was validated experimentally. Thus, a theoretical foundation was established for the development of Fe-based amorphous alloys, supporting the design of alloys with excellent GFA and high magnetic saturations.

Experimental and Simulation Methods. Alloy ingots with nominal compositions of $Fe_{86-x}Co_xB_7C_7$ (x = 0–10 at.%; denoted as Co_x), $Fe_{86-y}Ni_yB_7C_7$ (y = 0–10 at.%; denoted as Ni_y), and $Fe_{86-x-y}Co_XNi_yB_7C_7$ (x = 5, y = 3; x = 10, y = 3 and 5 at.%; denoted as Co_xNi_y) were prepared by induction melting of mixtures of pure Fe, Co, and Ni metals and pre-alloys of Fe-B and Fe-C in an argon atmosphere. The as-spun ribbons were then fabricated using the single-roller melt-spinning method with a linear velocity of 40 m/s in an argon atmosphere. These ribbons have a thickness of approximately 20 μm and a width of about 1 mm. The structure of the as-spun ribbons was characterized using X-ray diffraction (XRD DX-2700BH) with a Cu Kα source. The thermodynamic parameters of all the amorphous alloys were determined using differential scanning calorimetry (DSC 8000) and a simultaneous thermal analyzer (STA 8000) under argon flow at a heating rate of 10 K/min. The magnetization of the as-spun ribbons was measured at room temperature using a vibrating sample magnetometer (VSM) with a maximum applied field of 800 kA/m. AIMD simulations based on density functional theory (DFT) were performed using the Vienna *ab initio* simulation package (VASP).[27] The projected augmented wave (PAW) method was used to accurately describe the electron-ion interactions, and the generalized gradient approximation (GGA) was employed to effectively capture the exchange correlation among electrons.[28] Simulations were conducted in a canonical ensemble (NVT) with temperature control provided by a Nosé–Hoover thermostat. A cubic supercell with periodic boundary conditions containing 200 atoms was generated using the Monte Carlo method, and the supercell size was determined based on the alloy density at room temperature. Brillouin zone sampling was performed at the Γ point. The alloys were equilibrated for 1500 steps (2 fs for each step) at 1800 K to remove the memory from the initial configurations and then cooled to 1200 K and 300 K at a rate of 2×10^{14} K/s. A $3 \times 3 \times 3$ k-point mesh was used for accurate electron density of state (DOS) calculations. The DOS was calculated by considering the spin polarization, and an analysis of the DOS was used to determine the magnetic moments of the alloys.

Results and Discussion. The XRD patterns of the as-spun ribbons of $Fe_{86-x-y}Co_xNi_yB_7C_7$ (x = 0–10; y = 0–10 at.%) are presented in Fig. S1 in Supplementary Materials. All samples exhibit broad diffraction peaks at $2\theta \approx 45°$, with no distinct crystallization peaks observed, indicating that all ribbons have a fully amorphous structure. Figure 1 shows the DSC curves of the amorphous alloys. For the $Fe_{86}B_7C_7$ amorphous alloy, the DSC curve does not exhibit a distinct glass transition temperature (T_g) but displays a clear Curie temperature (T_c). The DSC curve shows a noticeable T_g upon the addition of Co or Ni. However, no T_c was observed in the DSC curves of the other alloys, probably because the addition of Co and Ni enhances the T_c of the alloy, resulting in T_c approaching or exceeding T_{x1}. The Bethe–Slater curve shows that the atomic exchange interaction between Fe–Co and Fe–Ni pairs is stronger than that between Fe–Fe pairs. Consequently, the addition of Co or Ni leads to the replacement of some Fe–Fe pairs with Fe–Co or Fe–Ni pairs, thereby enhancing the average atomic exchange interaction among the magnetic atoms and increasing the T_c of the alloy. Table 1 summarizes the thermodynamic parameters of all the amorphous alloys. Notably, T_g and T_{x1} increase initially with increasing Co content but then decrease. The addition of Ni significantly enhances both T_g and T_{x1}, particularly in the Ni_{10} alloy, for which their maximum values are observed. Moreover, codoping with Co and Ni has a relatively minor effect on the T_g and T_{x1} values of the alloy. To further evaluate the GFA of the alloys, the thermodynamic parameters ΔT ($T_{x1} - T_g$) and T_{rg} (T_g/T_l) were analyzed. The results are shown in Table 1, which indicate that the addition of Co and Ni

Table 1. Thermodynamic parameters of various amorphous alloys (T_g is the glass transition temperature, T_{x1} is the first crystallization temperature, T_{x2} is the second crystallization temperature, T_l is the melting temperature, $\Delta T = T_{x1} - T_g$, and $T_{rg} = T_g/T_l$).

Amorphous alloys	T_g (K)	T_{x1} (K)	T_{x2} (K)	T_l (K)	ΔT (K)	T_{rg}
$Fe_{86}B_7C_7$	–	621	743	1458	–	–
$Fe_{83}Co_3B_7C_7$	563	606	750	1394	43	0.404
$Fe_{81}Co_5B_7C_7$	561	603	745	1388	42	0.405
$Fe_{76}Co_{10}B_7C_7$	571	615	751	1374	44	0.416
$Fe_{83}Ni_3B_7C_7$	572	623	742	1392	51	0.411
$Fe_{81}Ni_5B_7C_7$	570	625	737	1389	57	0.410
$Fe_{76}Ni_{10}B_7C_7$	582	653	721	1368	71	0.425
$Fe_{78}Co_5Ni_3B_7C_7$	574	624	747	1386	50	0.414
$Fe_{73}Co_{10}Ni_3B_7C_7$	567	620	746	1382	53	0.410
$Fe_{71}Co_{10}Ni_5B_7C_7$	573	624	744	1376	51	0.416

leads to an increase in ΔT and T_{rg}, with Ni exerting a more pronounced influence on these parameters. This suggests that the addition of either Co or Ni enhances the GFA of the alloy, with the improvement being particularly pronounced for Ni. Among all the amorphous alloys, the Ni_{10} alloy is expected to exhibit the best GFA. To verify this, the critical thicknesses of $Fe_{86}B_7C_7$, Co_{10}, Ni_{10}, and Co_5Ni_3 alloys were measured by controlling the roll speed during preparation. The critical thicknesses were found to be 23, 32, 45, and 33 μm, respectively. This further demonstrates that the substitution of Fe with Co and Ni significantly enhances the GFA of the $Fe_{86}B_7C_7$ alloy.

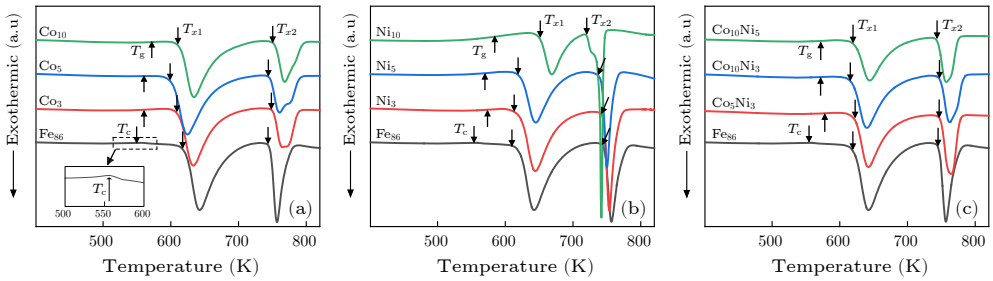

Fig. 1. DSC curves of various amorphous alloys: (a) $Fe_{86-x}Co_xB_7C_7$ (x = 0–10 at.%), (b) $Fe_{86-x}Ni_xB_7C_7$ (x = 0–10 at.%), (c) $Fe_{86-x-y}Co_XNi_yB_7C_7$ ($x = 5$, $y = 3$; $x = 10$, $y = 3$ and 5 at.%).

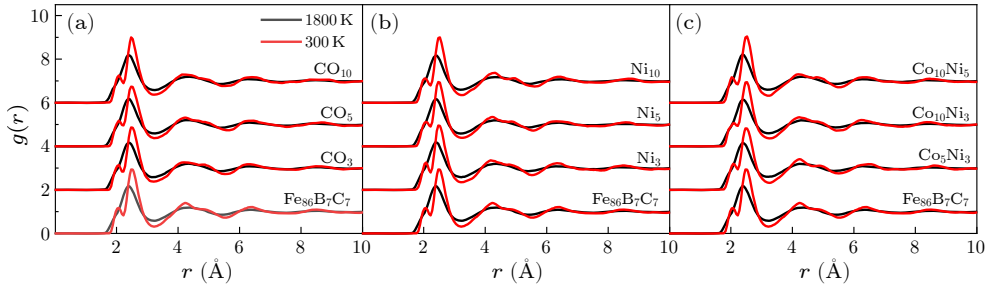

Fig. 2. Total PDFs of different alloys at 1800 K and 300 K: (a) $Fe_{86-x}Co_xB_7C_7$ (x = 0–10 at.%), (b) $Fe_{86-x}Ni_xB_7C_7$ (x = 0–10 at.%), (c) $Fe_{86-x-y}Co_XNi_yB_7C_7$ ($x = 5$, $y = 3$; $x = 10$, $y = 3$ and 5 at.%).

To investigate the influence of Co and Ni on the GFA of the alloys from an atomic structural perspective, various structural parameters were calculated, including the pair distribution function (PDF), Voronoi polyhedron (VP), and bond pairs. The commonly used form of the PDF is the Faber–Ziman form expressed as follows:[29]

$$g_{\alpha\beta}(r) = \frac{N}{4\pi^2\rho N_\alpha N_\beta}\sum_{i=1}^{N_\alpha}\sum_{j=1}^{N_\beta}\delta(r - r_{ij}), \quad (1)$$

where N is the total number of atoms, N_α and N_β are the numbers of atoms of types α and β, respectively, ρ is the atomic density, and r_{ij} is the distance between atoms i and j. Figure 2 presents the PDF curves of all alloys simulated at 1800 K and 300 K. As the temperature decreases, the height of the first peak increases, indicating enhanced short-range order. Moreover, the splitting of the second peak suggests the emergence of a mid-range order, providing evidence for the formation of amorphous structures in the AIMD simulations.[30] This splitting is typically attributed to uneven connectivity within the atomic clusters.[21] The transition from the liquid to the glassy state of the alloy is likely associated with a combination of increased local topological order and cluster connectivity formation, giving rise to the characteristic PDF curve.[31] Additionally, at 300 K, a minor sub-peak appeared on the left shoulder of the first peak in the PDF curves for all alloys. This sub-peak does not indicate crystallization but rather reflects the inconsistent positions of the first peak values for $g_{Fe-Fe}(r)$, $g_{Fe-B}(r)$, and $g_{Fe-C}(r)$.

Figure 3 displays the partial pair distribution function (PPDF) curves for $Fe_{86-x-y}Co_XNi_yB_7C_7$ ($x = 5$, $y = 3$; $x = 10$, $y = 3$ and 5 at.%) alloys at 1800 K and 300 K. As the PPDF curves of other alloys are similar, we present them in Figs. S2 and S3. The results indicate that the PPDF curves for Fe, Co, and Ni atoms are similar to the PDF curves of the alloys, with a higher first peak at 300 K and the second peak being split. The position of the first peak in the PPDF curve for Fe atoms shifts significantly to the right with increasing temperature, indicating changes in the bond length. This shift is attributed to the differences in bond lengths between Fe atoms in the ferromagnetic and paramagnetic states; specifically, the bond length of Fe atoms is greater in the ferromagnetic state than in the paramagnetic state, resulting in a corresponding shift in the position of the first peak of the PDF curve. Additionally, the first peak in the PPDF curves for the B and C atoms is less pronounced, suggesting better solute-solute avoidance.[32] This facilitates the formation of stable atomic clusters that stabilize the alloy in its molten and amorphous states, reduce compositional segregation, and ultimately improve the GFA of the alloy.

The bond lengths between the Fe, Co, and Ni atom pairs were inferred from the positions of the first peaks in the PPDF curves, as summarized in Table S1. To confirm whether chemical bonds were formed between these

atoms, we compared the positions of the first peaks with their atomic radii and sum of their radii (r_{sum}). The results show that the positions of the first peaks are consistently smaller than the corresponding sums of the atomic radii, suggesting the presence of covalent bonding between Fe, Co, and Ni atoms, as well as between these atoms and the B and C atoms. According to the Bethe–Slater curve, the bond length of Fe atoms affects their magnetic moments, with longer bond lengths generally corresponding to larger atomic magnetic moments within a certain range.[16] The addition of Co or Ni to the $Fe_{86}B_7C_7$ amorphous alloy increased the bond lengths of Fe atoms, indicating an enhancement in the magnetic moment of the Fe atoms. Among these alloys, the $Co_{10}Ni_5$ alloy is expected to exhibit the largest Fe atomic magnetic moment, which is advantageous for the magnetic properties of the alloys.

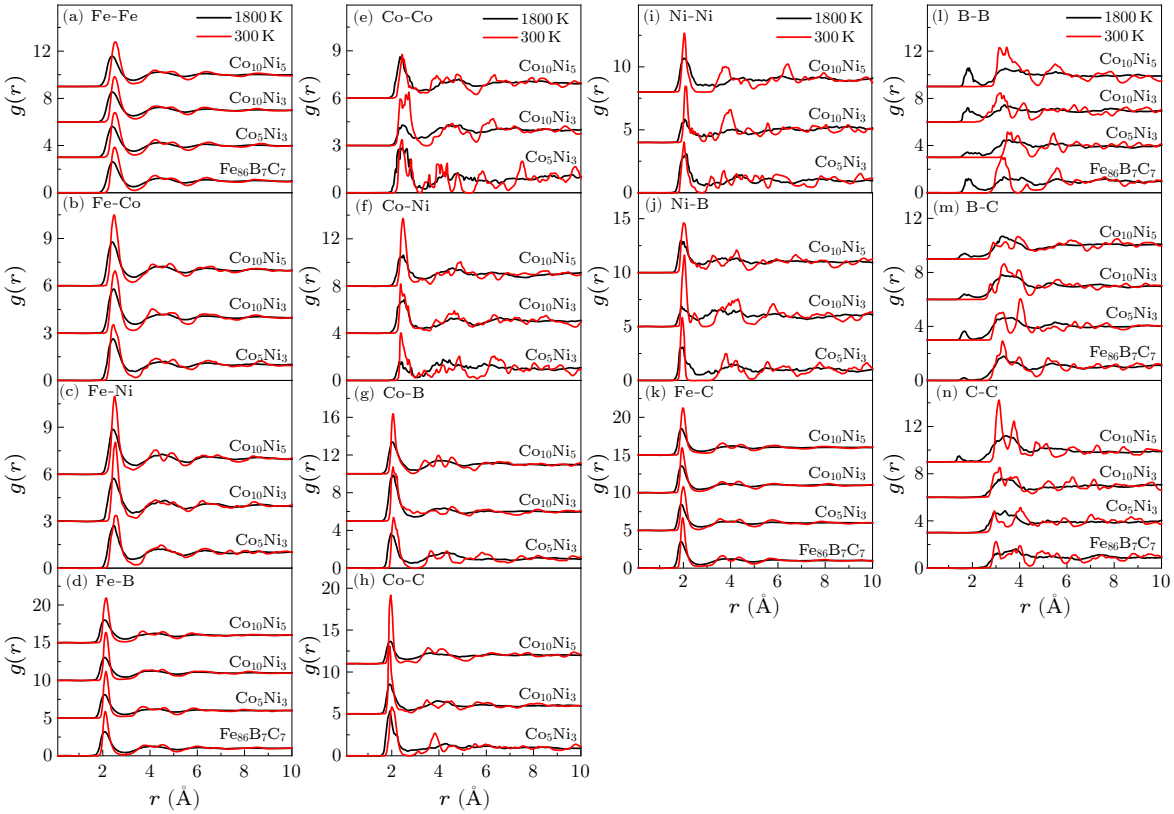

Fig. 3. PPDFs of $Fe_{86-x-y}Co_XNi_yB_7C_7$ ($x = 5$, $y = 3$; $x = 10$, $y = 3$ and 5 at.%) alloys at 1800 K and 300 K.

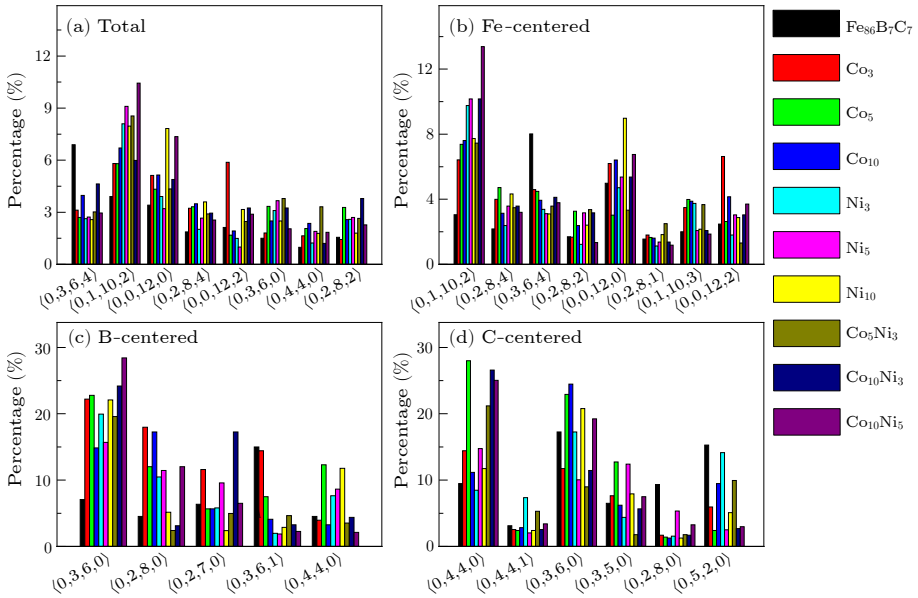

Fig. 4. Distribution of atomically centered VP polyhedra in various amorphous alloys: (a) total; (b) Fe-centered; (c) B-centered; (d) C-centered.

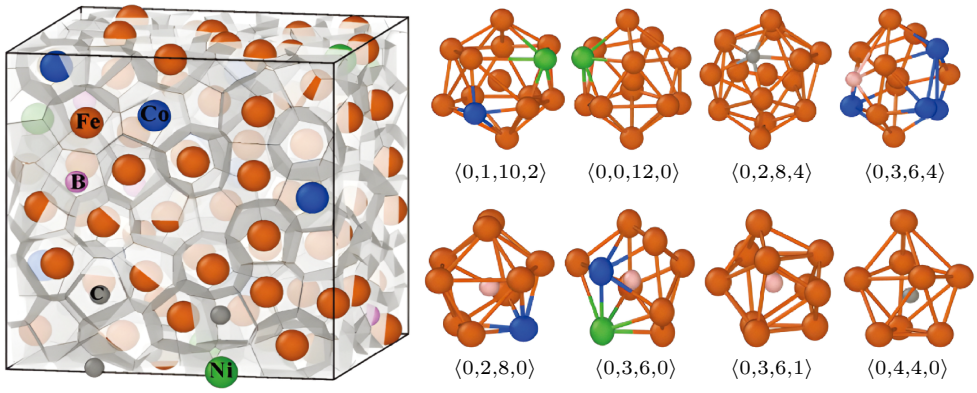

Fig. 5. Model of typical VPs in various amorphous alloys.

To further elucidate the local atomic structures of the amorphous alloys, we analyzed their major VPs at 300 K, as shown in Figs. 4 and 5. The VP index is defined as $\langle n_3, n_4, n_5, n_6\rangle$, where n_i represents the number of i-edged faces in the Voronoi polyhedron, and the sum of n_i provides the coordination number (CN) of the atom.[33] The analysis revealed that the Fe-centered polyhedra predominantly consisted of $\langle 0, 1, 10, 2\rangle$, $\langle 0, 0, 12, 0\rangle$, $\langle 0, 2, 8, 4\rangle$, $\langle 0, 3, 6, 4\rangle$, and $\langle 0, 2, 8, 2\rangle$. The polyhedra $\langle 0, 0, 12, 0\rangle$ correspond to perfect icosahedral structures, whereas $\langle 0, 1, 10, 2\rangle$ represent icosahedral-like structures, and $\langle 0, 3, 6, 4\rangle$ indicate a deformed body-centered cubic (bcc) structure, revealing a predominance of icosahedral-like and bcc clusters around the Fe atoms. The B-centered polyhedra mainly include $\langle 0, 3, 6, 0\rangle$ and $\langle 0, 3, 6, 1\rangle$, which correspond to tricapped trigonal prism (TTP) and distorted TTP structures, respectively, and $\langle 0, 2, 8, 0\rangle$ and $\langle 0, 4, 4, 0\rangle$, which represent Archimedean anti-prismatic structures. For C-centered polyhedra, in addition to the high frequency of $\langle 0, 4, 4, 0\rangle$ and $\langle 0, 3, 6, 0\rangle$ structures, various distorted TTP structures such as $\langle 0, 3, 5, 0\rangle$ and $\langle 0, 5, 2, 0\rangle$ are present. This indicates that the local structures around the B and C atoms in all the amorphous alloys are predominantly trigonal prismatic.

In general, owing to their five-fold symmetry, icosahedral structures tend to form dense atomic packing, thereby inhibiting periodic ordering and suppressing the nucleation of the crystalline phases.[30] Consequently, amorphous alloys with strong GFA typically exhibit a high content of icosahedral structures, as reflected in their coordination number distributions. Figure 6 illustrates the coordination number distribution of Fe atoms within all the amorphous alloys at 300 K, along with their average coordination numbers. The comparative results indicate that the average coordination number of the Fe atoms decreases with the addition of Co or Ni, suggesting the formation of more icosahedral clusters around the Fe atoms within the alloy. Such cluster structures are generally more stable and enhance the GFA of amorphous alloys.

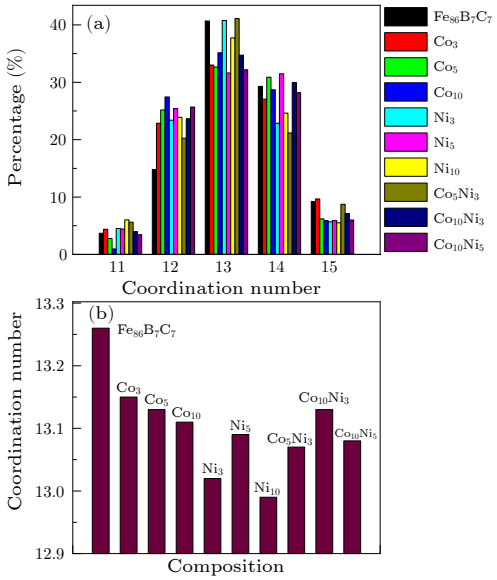

Fig. 6. (a) Distributions of coordination numbers in Fe-centered clusters in various amorphous alloys; (b) Average coordination number of Fe atoms in various amorphous alloys at 300 K.

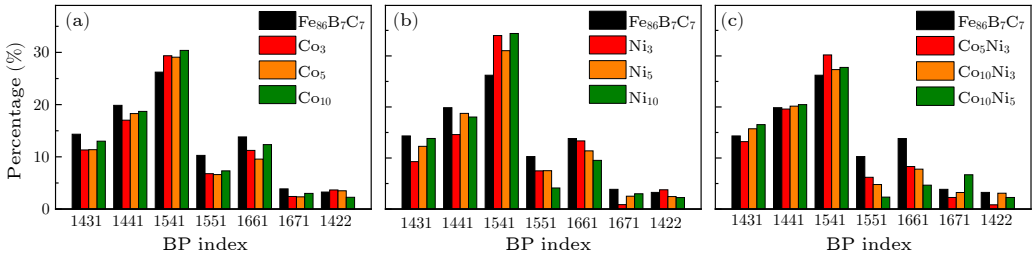

Fig. 7. Bond pair distributions of various alloys at 300 K: (a) $Fe_{86-x}Co_xB_7C_7$ (x = 0–10 at.%), (b) $Fe_{86-x}Ni_xB_7C_7$ (x = 0–10 at.%), (c) $Fe_{86-x-y}Co_XNi_yB_7C_7$ (x = 5, y = 3; x = 10, y = 3 and 5 at.%).

The atomic structural configurations of the alloys were further analyzed using the HA bond pair index method. The HA bond pair index utilizes four indices, i, j, k, and l, to describe the bonding interactions between pairs of atoms and their shared neighboring atoms.[34] According to the nearest neighbor of $g_{ij}(\mathrm{r})$, if atoms A and B form a bond, $i = 1$; otherwise, $i = 2$; j represents the number of neighboring atoms that form bonds with both atoms A and B; k denotes the number of bonds formed by these common neighbors; and l is a special classifying index. The bond pair distributions of all the alloys are shown in Fig. 7. The four compositions of the amorphous alloys consisted predominantly of 1541, 1551, 1431, 1441, and 1661 bond pairs. According to the HA index method, 1541, 1551, and 1431 bond pairs are associated with icosahedral structures, whereas 1441 and 1661 bond pairs correspond to bcc structures. The analysis reveals that the micro-structures of all the amorphous alloys considered in this study are primarily composed of icosahedral and bcc structures, with a significantly higher proportion of bond pairs associated with icosahedral structures than those associated with bcc structures.

As previously discussed, a high content of icosahedral structures and a low content of BCC structures are beneficial for enhancing the GFA of the alloys. To investigate this further, the ratios and discrepancies between the bond pairs corresponding to the icosahedral and bcc structures at 300 K were statistically analyzed, as illustrated in Fig. 8. The results indicate that the addition of Co or Ni significantly increases the difference between the contents of bond pairs corresponding to icosahedral and bcc structures, with the Ni_{10} composition showing the largest difference. This finding is consistent with previous experimental results, suggesting that the Ni_{10} alloy possesses an optimal GFA. Moreover, it highlights the close relationship between the good GFA in this series of alloys and the maintenance of a high content of icosahedral structures coupled with a low content of BCC structures.

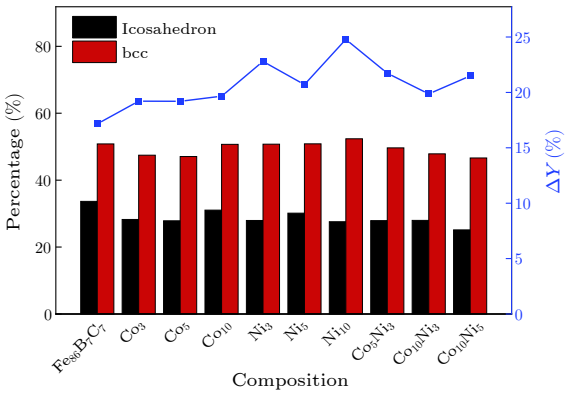

Fig. 8. Ratios of icosahedral and bcc polyhedra in various amorphous alloys at 300 K and their differences.

To investigate the effects of Co and Ni doping on the magnetic properties of the $Fe_{86}B_7C_7$ amorphous alloy, we conducted a detailed analysis of its electronic density of states (DOS) and magnetic moment. Figure 9(a) illustrates the total DOS of the $Fe_{86-x-y}Co_xNi_yB_7C_7$ (x = 0–10; y = 0–10 at.%) amorphous alloys, revealing that the total DOS is generally similar across all compositions and exhibiting a characteristic asymmetrical splitting of the spin-up and spin-down bands. This band splitting leads to different magnetic moments for the spin-up and spin-down electrons. When the Fermi level falls within the gap of the spin-down band (referred to as the pseudogap), pronounced ferromagnetism is observed in the amorphous alloy.[34] Previous research has indicated that a higher DOS near the Fermi level is associated with an increased number of non-bonding pairs in the system.[24,31] This phenomenon can weaken the interatomic interactions and diminish the stability of the local atomic structure. As depicted in Fig. 9(b), the $Fe_{86}B_7C_7$ alloy had the highest DOS value. In contrast, the DOS values of the Co_3, Co_5, and $Co_{10}Ni_5$ alloys were slightly lower than that of $Fe_{86}B_7C_7$, and the DOS values of the other compositions were even lower. These findings imply that the interatomic bonding in the Co_{10}, Ni_3, Ni_5, Ni_{10}, Co_5Ni_3, and $Co_{10}Ni_5$ amorphous alloys was stronger, facilitating the formation of a stable amorphous structure and enhancing the GFA.

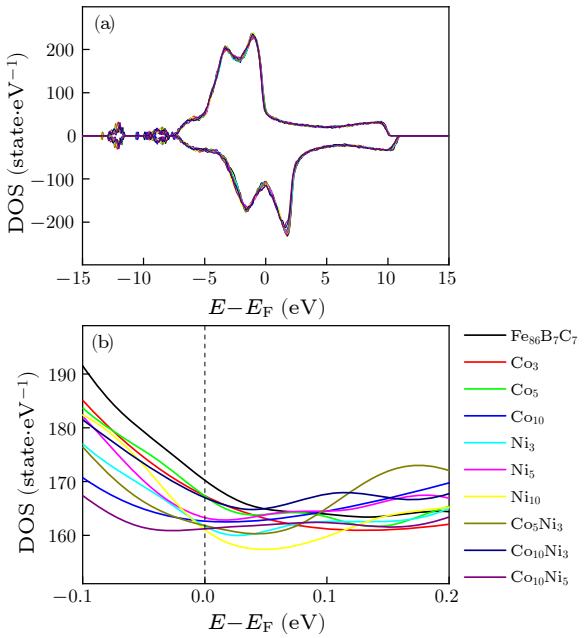

Fig. 9. (a) Total DOS of various amorphous alloys; (b) sum of electron state densities in the spin up and spin down orbits near the Fermi levels of various amorphous alloys.

Given the similarity in the DOS of Fe, Co, Ni, B, and C in all the amorphous alloys, we selected $Fe_{76}Co_{10}B_7C_7$, $Fe_{76}Ni_{10}B_7C_7$, and $Fe_{71}Co_{10}Ni_5B_7C_7$ for further analysis of their DOS, as shown in Fig. 10. The analysis reveals that the total DOS of these alloys is predominantly derived from the Fe-3d orbital electron states, with contributions from the Co-3d and Ni-3d orbitals being relatively minor. These orbitals are the primary contributors to the magnetic properties of the alloys. Additionally, hybridization between the Fe-3d, Co-3d, Ni-3d, and B-2p, C-2p orbitals

was observed. This interatomic orbital hybridization can modify the exchange energy or energy gap between orbitals, thereby facilitating the formation of bonds between atoms.[33] This finding suggests the existence of chemical bonds between these magnetic atoms and the B and C atoms, enhancing the structural stability and playing a critical role in glass formation.

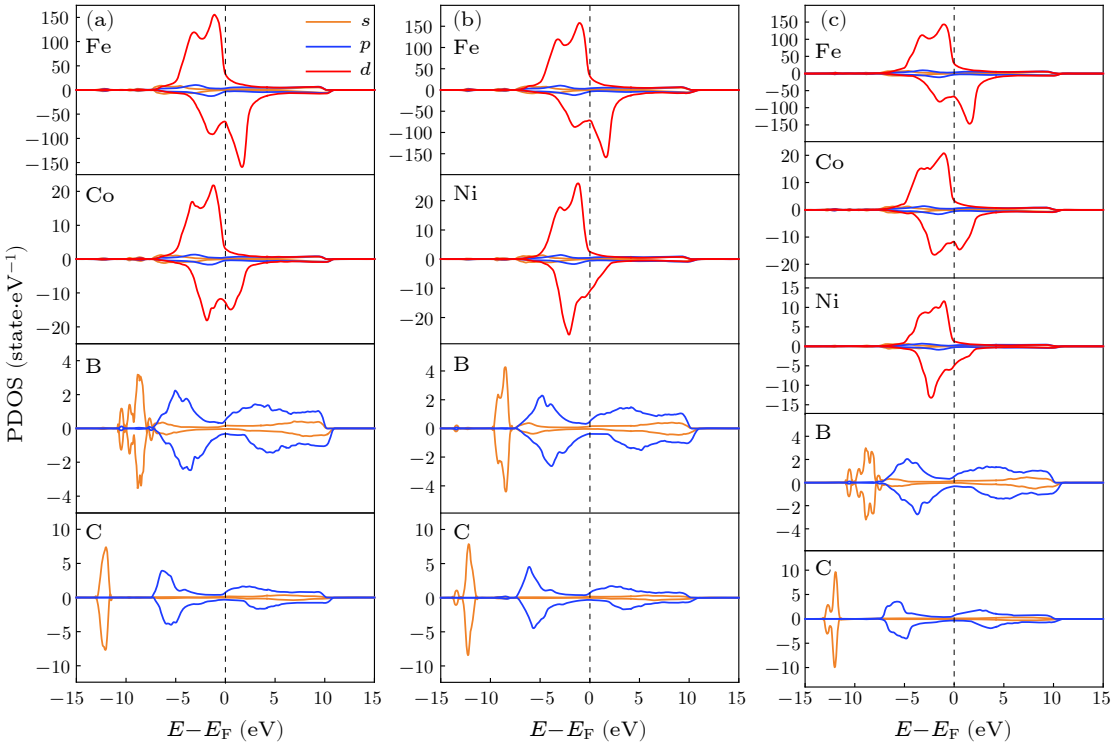

Fig. 10. PDOS of three amorphous alloys: (a) $Fe_7Co_{10}B_7C_7$, (b) $Fe_{76}Ni_{10}B_7C_7$, (c) $Fe_{71}Co_{10}Ni_5B_7C_7$.

Table 2. Calculated average total magnetic moments $M_{\mathrm{cal-total}}(\mu_B/\mathrm{atom})$ compared with the experimental values $M_{\mathrm{exp-total}}(\mu_B/\mathrm{atom})$ and average local magnetic moments (μ_B/atom) of various elements in the amorphous alloys.

Alloys	$M_{\mathrm{exp-total}}$	$M_{\mathrm{cal-total}}$	$m_{\mathrm{cal-Fe}}$	$m_{\mathrm{cal-Co}}$	$m_{\mathrm{cal-Ni}}$	$m_{\mathrm{cal-B}}$	$m_{\mathrm{cal-C}}$
$Fe_{86}B_7C_7$	1.605	1.815	2.135	–	–	−0.168	−0.137
$Fe_{83}Co_3B_7C_7$	1.623	1.839	2.195	1.336	–	−0.171	−0.146
$Fe_{81}Co_5B_7C_7$	1.653	1.853	2.226	1.404	–	−0.161	−0.138
$Fe_{76}Co_{10}B_7C_7$	1.672	1.865	2.282	1.497	–	−0.152	−0.128
$Fe_{83}Ni_3B_7C_7$	1.619	1.823	2.205	–	0.504	−0.171	−0.148
$Fe_{81}Ni_5B_7C_7$	1.596	1.808	2.225	–	0.546	−0.164	−0.141
$Fe_{76}Ni_{10}B_7C_7$	1.563	1.746	2.252	–	0.561	−0.158	−0.136
$Fe_{78}Co_5Ni_3B_7C_7$	1.675	1.845	2.275	1.521	0.484	−0.156	−0.135
$Fe_{73}Co_{10}Ni_3B_7C_7$	1.660	1.826	2.289	1.577	0.546	−0.158	−0.127
$Fe_{71}Co_{10}Ni_5B_7C_7$	1.648	1.797	2.298	1.547	0.576	−0.152	−0.127

Figure 10 also shows that the DOS of Co is similar to that of Fe, exhibiting a significant pseudogap and indicating that Co demonstrates a certain degree of ferromagnetism, with its atomic magnetic moment likely exceeding that of Ni. To further investigate the impact of these three magnetic elements on the magnetism of the alloy, we summarized the average atomic magnetic moments of all the amorphous alloys at 300 K in Table 2. The average magnetic moment of the Fe atoms in all the alloys exceeds $2\,\mu_B$, primarily contributed by the Fe-3d orbital magnetic moment. Meanwhile, both Co and Ni exhibit certain magnetic moments with the average atomic values approximately being $1.5\,\mu_B$ and $0.5\,\mu_B$, respectively. The contributions from B and C to the system's magnetic moment are minimal, with average values of approximately $-0.15\,\mu_B$ and $-0.13\,\mu_B$, respectively. The comparisons reveal that the average magnetic moment of Fe increases with the addition of Co and Ni. Both Co and Ni doping significantly enhance the magnetic moment of Fe atoms, with Co having a more pronounced effect than Ni. Moreover, the simultaneous introduction of Co and Ni further enhances the Fe magnetic moment, with its value reaching up to $2.3\,\mu_B$. Two factors contribute to the enhancement of the magnetic moment of the Fe atoms. First, upon the addition of Co and Ni, the Fe-3d electrons are redistributed between the spin-up and spin-down states in response to

changes in the number and type of nearest neighbors surrounding the Fe atoms,[25] as depicted in Fig. 6. Second, the exchange interactions between Fe–Co and Fe–Ni pairs are stronger than those between Fe–Fe pairs, resulting in an increase in T_c and enhancement of both the ferromagnetic properties of the alloys and the magnetic moment of the Fe atoms.[16]

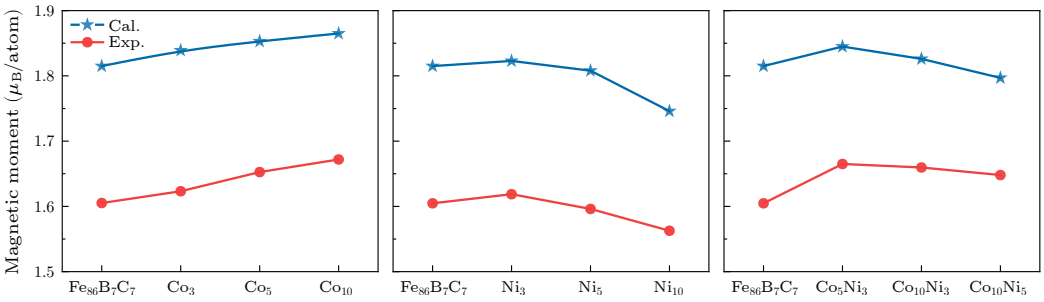

Fig. 11. Comparison of experimental and computational results for the magnetic moments of various amorphous alloys.

To clarify the influence of Co and Ni on magnetism, we analyzed the total magnetic moments of all amorphous alloys, as depicted in Fig. 11. The addition of Co results in a positive correlation between the total magnetic moment and Co content. In contrast, the total magnetic moment initially increases with the addition of Ni, before subsequently decreasing at higher Ni contents. When both Co and Ni are added, the total magnetic moment reaches its maximum for the Co_5Ni_3 alloy. However, excessive addition of Co and Ni can diminish the overall magnetic moment owing to diffusion effects, as this reduces the Fe content and contributes to a relatively lower magnetic moment. Because Co has a higher magnetic moment than Ni, in this study, both the Co and Ni contents were maintained below 10%, which ensured that the total magnetic moment did not decrease with increasing Co content. To validate the theoretical simulation results, we measured the average atomic magnetic moments of all the amorphous alloys, as shown in Fig. 11. The results indicate that the trends in the average atomic magnetic moments from both the simulation and experimental data are generally consistent, confirming that the appropriate addition of Co and a minor addition of Ni can enhance the total magnetic moment of the alloy.

The effect of ferromagnetic elements (Fe, Co, and Ni) on the microstructure and magnetic properties of Fe-based amorphous alloys was systematically investigated. Using AIMD simulations and experimental methods, we demonstrate that the addition of Co and Ni significantly changes the local structures of the alloys. This change in the local structure is characterized by an increased proportion of icosahedral structures and a decreased proportion of bcc structures, indicating enhanced structural stability, especially at a Ni content of 10%. This observation correlates with the experimentally observed improvement in GFA, highlighting the close relationship between GFA and icosahedral structure content. Furthermore, our simulation results demonstrate that Co and Ni doping effectively enhance the magnetic moment of Fe atoms owing to the redistribution of the Fe-3*d* charge between the spin-up and spin-down states in response to changes in the local environment surrounding the Fe atoms as well as the strong exchange interactions of Fe–Co and Fe–Ni pairs. The experimental results corroborate these findings, indicating that the appropriate addition of Co and a minor addition of Ni can significantly enhance the total magnetic moment of the alloy. Overall, this study provides critical insight into the optimization of Fe-based amorphous alloys and paves the way for the development of high-performance magnetic materials.

Acknowledgment. This work was supported by the National Natural Science Foundation of China under Grant No. 10225417 and the National Basic Research Program of China under Grant No. 2006CB601003.

References

[1] Li H X, Lu Z C, Wang S L, Wu Y, and Lu Z P 2019 *Prog. Mater. Sci.* **103** 235
[2] Silveyra J M, Ferrara E, Huber D L, and Monson T C 2018 *Science* **362** eaao0195
[3] Wang W H, Dong C, and Shek C H 2004 *Mater. Sci. Eng. R* **44** 45
[4] Seghairi N, Bendjemil B, Lavorato G, Castellero A, and Baricco M 2012 *Chin. Phys. Lett.* **29** 118102
[5] Huo J, Li K, Zang B, Gao M, Wang L M, Sun B, Li M, Song L, Wang J Q, and Wang W H 2022 *Chin. Phys. Lett.* **39** 046401
[6] Ohta M and Hasegawa R 2017 *IEEE Trans. Magn.* **53** 2000205
[7] Kasai S, Namikawa M, and Hiratani T 2016 *JFE Tech. Rep.* **21** 14
[8] Shi L and Yao K 2020 *Mater. Des.* **189** 108511
[9] Ri M C, Ding D W, Sun B A, Wang J Q, Zhu X S, Wang B B, Wang T L, Qiu Q Q, Huo L S, and Wang W H 2018 *Journal of Non-Crystalline Solids* **495** 54
[10] Qi Z G, Chen Q, Wang Z X, Song Z Q, Kim K B, Pang J, Zhang X H, and Wang W M 2024 *npj Mater. Degrad.* **8** 28
[11] Duan X Y, Ju S W, Li Y H, Zhu Z W, Zhang H F, and Zhang W 2023 *J. Non-Cryst. Solids* **616** 122480
[12] Qi X J, You J H, Zhou J F, Qiu K Q, Cui X L, Tian J, and Li B L 2023 *Phys. Status Solidi* **220** 2300079
[13] Shi L, Hu X, Li Y, Yuan G, and Yao K 2021 *Intermetallics* **131** 107116

[14] Xiao J H, Ding D W, Li L, Sun Y T, Li M Z, and Wang W H 2024 *Chin. Phys. B* **33** 076101
[15] Hou L, Fan X, Wang Q, Yang W, and Shen B 2019 *J. Mater. Sci. Technol.* **35** 1655
[16] Li X, Zhou J, Shen L, Sun B, Bai H, and Wang W 2023 *Adv. Mater.* **35** 2205863
[17] Wang F, Inoue A, Han Y, Zhu S L, Kong F L, Zanaeva E, Liu G D, Shalaan E, Al-Marzouki F, and Obaid A 2017 *J. Alloys Compd.* **723** 376
[18] Yang W, Liu H, Zhao Y, Inoue A, Jiang K, Huo J, Ling H, Li Q, and Shen B 2014 *Sci. Rep.* **4** 6233
[19] Chen P B, Liu T, Kong F Y, Wang A D, Yu C Y, Wang G, Chang C T, and Wang X M 2018 *J. Mater. Sci. Technol.* **34** 793
[20] Yu Q, Wang X D, Lou H B, Cao Q P, and Jiang J Z 2016 *Acta Mater.* **102** 116
[21] Ding J, Ma E, Asta M, and Ritchie R O 2015 *Sci. Rep.* **5** 17429
[22] Yuan C C, Deng C, Zhang H P, Li M Z, and Shen B L 2019 *Intermetallics* **112** 106501
[23] Ma H J, Shen K C, Pan S P, Zhao J, Qin J Y, Kim K B, and Wang W M 2015 *Journal of Non-Crystalline Solids* **425** 67
[24] Huang Z, Zhang Y, Shi R, Fu P, Zhu W, Tao P, Dong H, and Yang Y 2024 *Mater. Today Commun.* **39** 108604
[25] O'Handley R C and Boudreaux D S 1978 *Phys. Status Solidi A* **45** 607
[26] Tong X, Zhang Y E, Shang B S, Zhang H P, Li Z, Zhang Y, Wang G, Liu Y H, Zhao Y, Zhang B, Ke H B, Zhou J, Bai H Y, and Wang W H 2024 *Nat. Mater.* **23** 1193
[27] Kresse G and Joubert D 1999 *Phys. Rev. B* **59** 1758
[28] Blöchl P E 1994 *Phys. Rev. B* **50** 17953
[29] Faber T E and Ziman J M 1965 *Philos. Mag.* **11** 153
[30] Ma S, Ran Y, Liang X, Jiang L, Li Y, Wang X, Yao M, and Zhang W 2022 *J. Alloys Compd.* **902** 163637
[31] Jiang J, Li Q, Duan H, and Li H 2017 *Comput. Mater. Sci.* **130** 76
[32] Wang Y C, Zhang Y, Makino A, Liang Y Y, and Kawazoe Y 2014 *IEEE Trans. Magn.* **50** 2003704
[33] Finney J L 1977 *Nature* **266** 309
[34] Honeycutt J D and Andersen H C 1987 *J. Phys. Chem.* **91** 4950